Research Article Vol. 5, No. 9 / September 2018 / Optica 1099

Rotating black hole geometries in a two-dimensional photon superfluid

David Vocke,[1] Calum Maitland,[1,2] Angus Prain,[1,2] Kali E. Wilson,[1] Fabio Biancalana,[1] Ewan M. Wright,[1,3] Francesco Marino,[4,5] and Daniele Faccio[2,3,*]

[1]Institute of Photonics and Quantum Sciences, Heriot-Watt University, Edinburgh EH14 4AS, UK
[2]School of Physics and Astronomy, Kelvin Building, University of Glasgow, Glasgow G12 8QQ, UK
[3]College of Optical Sciences, University of Arizona, Tucson, Arizona 85721, USA
[4]CNR-Istituto Nazionale di Ottica, L.go E. Fermi 6, I-50125 Firenze, Italy
[5]INFN, Sez. di Firenze, Via Sansone 1, I-50019 Sesto Fiorentino (FI), Italy
*Corresponding author: Daniele.Faccio@glasgow.ac.uk

Received 29 March 2018; revised 30 July 2018; accepted 9 August 2018 (Doc. ID 326919); published 10 September 2018

Photon fluids have recently found applications in the simulation of a variety of physical phenomena such as superfluidity, vortex instabilities, and artificial gauge theories. Here we experimentally demonstrate the use of a photon fluid for analog gravity, i.e., the study of the physics of curved spacetime in the laboratory. While most analog gravity experiments are performed in 1 + 1 dimensions (one spatial plus time) and thus can only mimic 1 + 1D spacetime, we present a (room-temperature) photon superfluid where the geometry of a rotating acoustic black hole can be realized in 2 + 1D dimensions by an optical vortex. By measuring the local flow velocity and speed of waves in the photon superfluid, we identify a 2D region surrounded by an ergosphere and a spatially separated horizon.

OCIS codes: (160.6840) Thermo-optical materials; (190.0190) Nonlinear optics; (190.3270) Kerr effect; (190.4870) Photothermal effects; (350.5720) Relativity.
https://doi.org/10.1364/OPTICA.5.001099

1. INTRODUCTION

Photon fluids are nonlinear optical systems in which small perturbations in the transverse plane of a beam propagating in a nonlinear defocusing medium are described by the hydrodynamical Euler equations [1–4]. These equations contain an additional term due to diffraction that is completely analogous to the quantum pressure term that arises in the same equations describing a two-dimensional Bose–Einstein condensate (BEC). Photon fluids therefore form part of the larger family of so-called "quantum fluids of light" that also include polariton fluids and recent experiments on photon condensation [5–7].

Photon fluid density, which defines the speed of linear excitations (referred to as "sound" waves, in analogy to their BEC counterpart) is determined by the laser intensity, while the overall flow is controlled via the gradient of the spatial phase profile. This last aspect makes these systems extremely versatile as the spatial profile of a laser beam can be readily manipulated in amplitude and phase, thus enabling recent studies investigating, for example, superfluidity and vortex instabiities [4,8,9], artificial magnetic fields [10], and proposals for studying artificial spacetimes [11–16].

The field of analog gravity has demonstrated that the physics of curved spacetime can be studied in laboratory environments that exploit the formal analogy between waves in inhomogeneous fluid flows and scalar fields in curved spacetime [17–21]. In this context, a spatially varying flow maps onto an effective spacetime metric in which perturbative excitations, i.e., density or surface waves propagate. A horizon is formed at a surface where the flow speed across that surface exceeds the wave propagation speed, and hence, waves are blocked or trapped beyond that boundary.

Analog horizons have been realized in various systems, where quantum fluids such as BECs and classical systems such as surface waves in water or pulses of light in an optical medium play the most prominent roles [5,22–31]. These studies involved one-dimensional flow geometries and have had considerable success. The challenging realization of higher dimensional analog horizons has only recently being undertaken [32] and would enable the study of the effects of rotating spacetimes, for example, by setting the background flow into rotation similar to a vortex in a draining bathtub.

A rotating spacetime may form an ergosphere enclosing the internal region within which it is impossible for an observer to remain stationary relative to a distant observer. Recent experiments using draining water tanks showed that waves entering a hydrodynamic vortex may be scattered and amplified [32], effectively extracting rotational energy. This effect is related to a particle scattering effect first predicted by Penrose in 1969 [33–35] referred to as the Penrose process. A remarkably similar phenomenon, the Zel'dovich effect, appears in the context of

electromagnetic waves incident on rotating conducting or absorbing cylinders [36]. Related to this, the experimental realization of a 2 + 1D vortex flow with the identification of both a horizon and ergosphere has never been achieved so far.

In this work, following the theoretical prescription of Marino for realizing a rotating black hole geometry [37] in which it may be possible to observe the Penrose process [11], we use a room-temperature photon superfluid to create a 2 + 1D rotating spacetime with an inward draining radial flow. Measurements of the fluid density (i.e., wave speed) and phase gradients (i.e., flow speeds) along the radial and angular directions allow us to precisely identify the horizon and ergosphere location in the superfluid. The horizon is here analogous to the absorbing boundary of the conducting cylinder in Zel'dovich's original problem.

2. MODEL

Our photon fluid involves a monochromatic laser beam that propagates through a bulk medium with a thermo-optic nonlinearity [38,39]. In the paraxial approximation, the slowly varying envelope of the electric field $E(\mathbf{r}, z)$ with $\mathbf{r} = (x, y)$ is governed by the nonlinear Schrödinger equation (NLSE),

$$\partial_z E = \frac{i}{2k}\nabla_\perp^2 E + i\frac{k}{n_0}\Delta n E, \tag{1}$$

where z is the propagation direction, and $k = 2\pi n_0/\lambda$ is the longitudinal wave number. The nonlinear change of refractive index due to the thermo-optic response is described by

$$\Delta n = \gamma \iint \mathrm{d}r'\mathrm{d}z' R(r - r', z - z')|E(r', z')|^2, \tag{2}$$

where γ is the nonlinearity coefficient, and $R(r, z)$ is the nonlocal response function that will typically have an exponential-like decay in the transverse radial direction with spatial extent σ, which accounts for heat diffusion resulting from the absorbed laser power. If heat diffusion is sufficiently limited, i.e., $\sigma < \Lambda$ where Λ is the sound wavelength, then the nonlocal response function can be approximated as local, $R(r - r', z - z') = \delta(r - r', z - z')$, and thus, $\Delta n = \gamma|E(r, z)|^2$, where γ in our case is taken to be -4.4×10^{-7} cm^2/W (see below). We will later see that this is a valid assumption for the length scales considered in the experiments.

For a defocusing nonlinearity, i.e., $\Delta n < 0$, the NLSE can be recast in a set of hydrodynamical equations by means of the Madelung transform $E(r, t) = \sqrt{\rho(r, t)}e^{i\phi(r,t)}$ [2,12], as is also found for dilute BECs [40]

$$\partial_t \rho + \nabla(\rho v) = 0, \tag{3}$$

$$\partial_t \psi + \frac{1}{2}v^2 + \frac{c^2\gamma}{n_0^3}\rho - \frac{c^2}{2k^2 n_0^2}\frac{\nabla^2\sqrt{\rho}}{\sqrt{\rho}} = 0, \tag{4}$$

where the propagation axis is mapped onto a time coordinate, $t = zn_0/c$; the transverse phase gradient determines the fluid flow, $\mathbf{v}(r, t) = (c/kn_0)\nabla_\perp\phi(r, t) = \nabla_\perp\psi(r, t)$; and the laser intensity (equivalently the fluid density ρ) determines the speed of sound, $c_s(r, t) = \sqrt{c^2|\gamma|\rho(r, t)/n_0^3}$. Therefore, in the presence of repulsive nonlinear interactions, the transverse beam profile follows the mean-field dynamics of a BEC with the optical field E playing the role of the complex order parameter. An equation of motion for sound waves can then be obtained by linearizing Eqs. (3) and (4) around a stationary background solution, where elementary excitations are understood as first-order fluctuations of the optical field amplitude and phase, i.e., $\rho = \rho_0 + \rho_1$ and $\psi = \psi_0 + \psi_1$ with $\rho_1 \ll \rho_0$ and $\psi_1 \ll \psi_0$. The last term in Eq. (4) is the quantum pressure; it appears in optics due to diffraction and can be neglected in the hydrodynamic limit that is valid for length scales much larger than the healing length, $\zeta = \lambda/\sqrt{4n_0|\gamma|\rho}$. Typically, in our system this implies sound waves with wavelengths $\geq$300 μm [3]. In this case, the equation of motion for the phase perturbations can be written as a Klein–Gordon equation for a massless scalar field on a curved spacetime [37] with a spacetime metric $g_{\mu\nu}$ given by

$$g_{\mu\nu} = \left(\frac{\rho_0}{c_s}\right)^2 \begin{pmatrix} -(c_s^2 - v^2) & -v_r & -rv_\theta \\ -v_r & 1 & 0 \\ -rv_\theta & 0 & r^2 \end{pmatrix} \tag{5}$$

and $\mathbf{g} = \det(g_{\mu\nu})$. Here, v_r and v_θ are the radial and azimuthal velocity components, from which the total speed is $\mathbf{v}^2 = v_r^2 + v_\theta^2$. The speeds v_i and c_s are functions of the transverse coordinates, and hence, by tailoring the spatial phase and intensity profile it is possible to generate a family of (2 + 1) dimensional spacetime metrics.

Following the initial proposal by Marino [37], we create a rotating spacetime by using background vortex beams with orbital angular momentum (OAM) $E_0 = \sqrt{\rho_0(r)}\exp(im\theta)$, with topological charge integer m. The azimuthal fluid flow $v_\theta(r) = cm/(kn_0 r)$ is therefore proportional as a function of r to the topological charge of the beam. An ergosphere can then be created by controlling the beam intensity such that the speed of sound passes from faster to slower than the total flow. Any sonic observer within this region is forced to co-rotate with the flow due to the associated "superluminal" dragging of inertial frames. In order to create a trapped surface and thus an (apparent) horizon, an additional radial phase dependence must be imposed. In any region where the flow is inward-pointing and $|v_r| > c_s$, a sound wave will be swept inward by the fluid flow and be trapped inside the horizon that is formed where $|v_r| = c_s$.

Figure 1(a) shows the calculated absolute flow amplitudes and corresponding sound speed for a beam with initial amplitude

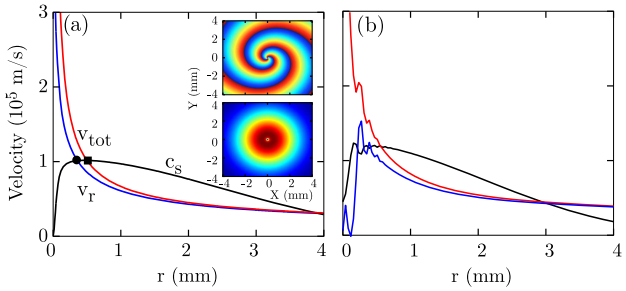

Fig. 1. (a) Initial flow and sound wave velocities calculated for a photon fluid with Gaussian intensity envelope (width $w_{1/e^2} =$ 5 mm, $P = 140$ mW, $|\gamma| = 4.4 \times 10^{-7}$ cm^2/W) and field amplitude $E_0 = \sqrt{\rho_0(r)}\exp(im\theta - 2i\pi\sqrt{r/r_0})$ with $r_0 = 0.5$ mm and $m = 2$. Total flow $v_{tot} = \sqrt{v_r^2 + v_\theta^2}$ (red), radial flow v_r (blue), and sound speed c_s (black) are shown. The solid circle (square) indicates the location of the horizon (ergosphere). Inset top: 2D phase profile with values from 0 (blue) to 2π (red). Inset bottom: near-field intensity profile (arb. units). (b) Flow and sound wave velocities after 13 cm propagation in a nonlocal nonlinear medium with the same parameters obtained from numerical integration of the NLSE [Eq. (1)].

$E_0 = \sqrt{\rho_0(r)}\exp(im\theta + i\phi(r))$, with Gaussian intensity envelope $\rho_0(r) = \rho_0\exp(-2r^2/\sigma^2)$ and radial phase $\phi(r) = -2\pi\sqrt{r/r_0}$ (which, upon propagation, will form a ring-shaped beam due to the phase singularity at $r = 0$). The radial phase induces a flow, $v_r(r) \propto \frac{\partial\phi}{\partial r} = -\pi/\sqrt{r_0 r}$. Figure 1(b) shows the same input beam propagated over a distance of 13 cm by numerically solving the NLSE using a split-step Fourier method (details of this standard numerical method can be found in [4]). The oscillations and modifications on the beam observed in Fig. 1(b) (e.g., small oscillations towards the center) are due to diffraction effects related to the inward radial phase or, in the quantum fluid language, are due to the inward flow accumulating towards the center of the vortex.

From the flows and the metric in Eq. (5), one can then calculate a set of quantities that are of central importance for establishing the validity of the fluid in terms of providing a correct analog of sonic propagation on a curved background [41]. First, the analog *surface gravity* is a measure of the effective mass of the black hole [19,20],

$$\kappa := \frac{1}{2}\partial_r(c_s^2 - v_r^2)|_{\text{horizon}}. \tag{6}$$

For the parameters used in Fig. 1, $\langle\kappa\rangle \simeq 1.74\times10^{13}$ ms^{-2}, which corresponds to phonons of wavelength $\lambda = c_s^2/\kappa \simeq 1$ mm that are longer than the healing length of 300 μm, and hence, in the sonic regime in which the spacetime description is valid. This parameter also occupies a central role in the Hawking process for analog black holes [42,43].

Second, in the Zel'dovich effect, the *angular velocity of the absorbing boundary* (here represented by the horizon) is the most relevant parameter, setting the frequencies of the most efficiently amplified modes through

$$\omega_Z \simeq \frac{v_\theta(r_H)}{r_H}, \tag{7}$$

where r_H is the location of the horizon (solid circle in Fig. 1). Again, for the parameters of Fig. 1, we find $\langle\omega_Z\rangle \simeq 2.03\times10^8$ s^{-1}, which corresponds to phonons with $\lambda = 2\pi c_s/\omega_Z \simeq 1$ mm, well within the sonic regime.

Third, we estimate the time scale of the evolution of the surface gravity as a measure of the evolution of the background through the experiment,

$$\tau^{-1} := \frac{\dot\kappa}{\kappa} \simeq \frac{|\kappa_f - \kappa_i|}{\Delta t}\frac{1}{\langle\kappa\rangle}. \tag{8}$$

Using the data of Fig. 1, we find $\tau^{-1} \simeq 1.04\times10^9$ s^{-1} corresponding to a wavelength of $\lambda = 2\pi c_s\tau \simeq 1$ mm; shorter wavelength phonons will perceive the background to evolve adiabatically.

Therefore, the window of modes for which the black hole is adiabatically evolving while still being in the sonic regime is $\lambda = 0.3$ – 1 mm, and this window overlaps with the set of efficiently amplifying modes controlled by ω_Z and mode conversion at the horizon, which is controlled by κ.

3. EXPERIMENTS

The experimental layout is shown in Fig. 2: a broad CW laser beam with Gaussian profile and vacuum wavelength $\lambda =$ 532 nm that is launched through a diffractive phase mask on a fused silica glass substrate, which is designed such that the first diffracted order carries the desired phase $\phi = m\theta - 2\pi\sqrt{r/r_0}$

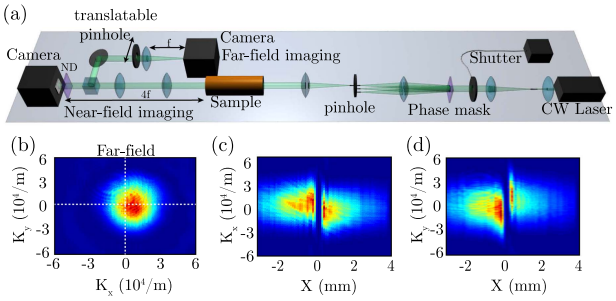

Fig. 2. (a) Experimental setup: a continuous-wave (CW) 532 nm laser beam is launched onto a diffractive phase mask, which imprints the desired phase. Diffracted orders are selected by a spatial filter in the focus of a $4f$-imaging telescope. A mechanical shutter shuts the beam on/off, which is then launched through a 13 cm long tube filled with a nonlinear methanol graphene solution. The near-field and far-field intensities are imaged at the output facet of the sample onto a CCD camera. The spatially resolved far field is recorded by selecting small areas of the near field by an iris ($\varnothing \approx 200$ μm) that is scanned across the beam diameter. (b) Example of the spatially selected far field. The location ($K_x(x, y = 0)$, $K_y(x, y = 0)$) of the spot, i.e., the central peak in the far field obtained by filtering the near field with the iris for varying horizontal iris position x at a fixed vertical position $y = 0$, is tracked during the scan to obtain the flow velocity. (c) and (d) Lineouts of far-field images (b) along the $K_y = 0$ and $K_x = 0$ axes (dotted white crosshair), respectively, as a function of iris position x.

with $m = 2$ and $r_0 = 0.5$ mm. The beam is then imaged shortly after the phase mask by a $4f$-imaging system onto the input facet of the nonlinear sample, so that the +1 and −1 orders can be selected by a pinhole in the far field of the first lens, thus selecting an $m = 2$ radial ingoing flow (black hole) or $m = -2$ outgoing flow (white hole). The sample consists of a cylindrical cell with length $L = 13$ cm and radius $W = 1$ cm filled with a dilute methanol/graphene solution as a nonlinear medium [3]. Finally, the near- and far-field intensities at the output facet of the nonlinear sample are recorded by a charge-coupled device (CCD) camera. Methanol provides a thermal defocusing nonlinearity induced by absorbed laser power $\Delta n(r) = \beta\Delta T(r)$ with a thermo-optic coefficient $\beta = -4\times10^{-4}$ 1/K while nanometric graphene flakes are added to increase absorption to ≈25% along propagation in order to provide sufficient nonlinearity. As mentioned above, heat diffusion in the transverse directions smears out the photon–photon interaction with a spatial extent described by the nonlocal length σ. By performing measurements after a short 200 ms time delay from the opening of the laser shutter, and with an exposure time of 20 ms on the camera, we effectively observe the evolution of the beam with a sufficiently high nonlinearity measured ([4,44]) to be $|\gamma| = 4.4\times10^{-7}$ cm^2/W with a measured nonlocal length less than 166 μm, i.e., smaller than the healing length, which can thus be ignored for the purpose of the experiments presented here.

The photon fluid flow is proportional to the gradient of the spatial phase and can be expressed as

$$\begin{pmatrix} v_x(r) \\ v_y(r) \end{pmatrix} = \frac{c}{n_0 k_0}\nabla\phi(r) = \frac{c}{n_0 k_0}\begin{pmatrix} K_x(r) \\ K_y(r) \end{pmatrix}. \tag{9}$$

This expression highlights that the local flow can be measured by recording the spatially resolved components $K_{x,y}(r)$ in the far field. This is performed by isolating points of the beam in the

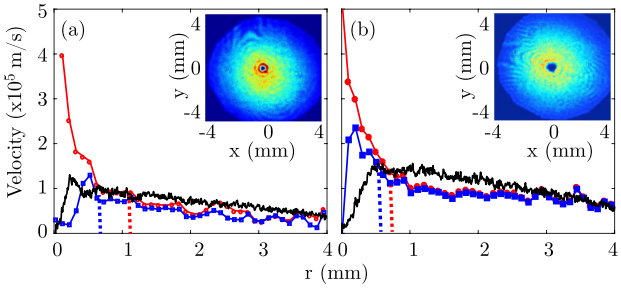

Fig. 3. (a) Black hole with experimental parameters $r_0 = 0.5$ mm, $m = 2$, $P = 140$ mW, $t = 200$ ms. (b) White hole with the same parameters and $t = 600$ ms. Experimental data shown are radial and total flow velocities (blue squares/line and red circles/line) and speed of sound (black) after propagation through 13 cm of methanol-graphene solution. Error bars are smaller than the data symbols and are therefore not shown. The horizon $[v_{\mathrm{tot}}(r) = c_s(r)]$ and ergosphere $[v_r(r) = c_s(r)]$ are shown with blue and red dotted lines, respectively. Inset: near-field intensity distribution at the sample output. The color code shows the intensity from 0 (dark blue) to 1 W/cm^2 (dark red).

near field with an aperture ($\varnothing \approx 200$ μm) and measuring the location $(K_x(r), K_y(r))$ of the intensity peaks in the far field (focal plane of a lens). The absolute values of the measured flows as well as the speed of sound are shown in Fig. 3(a) for a rotating black hole and Fig. 3(b) for a rotating white hole. An acoustic horizon can be identified in both cases at the intersection of the radial flow v_r (blue squares) and speed of sound c_s (solid black line) at $r \approx 0.5$ mm. The ergosphere is found at a larger radius than the horizon where the total flow $v_{\mathrm{tot}}^2 = v_r^2 + v_\theta^2$ intersects the sound speed. These measurements therefore completely identify the metric of the rotating photon fluid at the output plane. We note that Fig. 1 shows simulations performed under the same conditions as the experiment in Fig. 3(a) and shows a very good agreement in both the overall geometries (fluid flows and sound speed) and location of the horizon and ergosphere.

4. CONCLUSIONS

We have shown how, by shaping the input phase profile of a photon fluid, it is possible to create a rotating black-hole-like spacetime over a broad range of wavelengths. We have investigated in detail the main features of the effective rotating spacetime metric by comparing relevant length scales related to the surface gravity and amplified/scattered frequencies. These are of the order of or shorter than the length of the sample, hence indicating that much longer propagation lengths would be required in order to perform measurements of scattered wave amplitudes when these have reached asymptotically flat spacetime regions, as required for a full analogy with Penrose scattering. A tightly related process, Zel'dovich scattering from the boundary of an absorbing cylinder does not require such restrictions, and we can identify the absorbing boundary of the rotating cylinder with the spacetime horizon measured in the photon fluid. The close vicinity of the horizon and ergosphere in our setting effectively implies the co-location of the loss boundary (horizon) and energy extraction boundary (ergosphere) as in the original Zel'dovich problem. These experimental results therefore highlight how 2D + 1 spacetimes can be readily created in photon fluids with applications such as the study of Penrose-like and Zel'dovich amplification processes in future experiments.

Funding. H2020 European Research Council (ERC) (ERC GA 306559); H2020 Marie Skłodowska-Curie Actions (MSCA) (659301); Engineering and Physical Sciences Research Council (EPSRC) (EP/L015110/1, EP/M009122/1).

Acknowledgment. D.F. and A.P. acknowledge financial support from the European Research Council under the European Union Seventh Framework Programme, Marie Skłodowska-Curie and EPSRC. C.M. acknowledges studentship funding from EPSRC under CM-CDT. All data relevant to this work may be obtained at [45].

REFERENCES

1. T. Frisch, Y. Pomeau, and S. Rica, "Transition to dissipation in a model of superflow," Phys. Rev. Lett. **69**, 1644–1647 (1992).
2. R. Y. Chiao and J. Boyce, "Bogoliubov dispersion relation and the possibility of superfluidity for weakly interacting photons in a two-dimensional photon fluid," Phys. Rev. A **60**, 4114–4121 (1999).
3. D. Vocke, T. Roger, F. Marino, E. M. Wright, I. Carusotto, M. Clerici, and D. Faccio, "Experimental characterization of nonlocal photon fluids," Optica **2**, 484–490 (2015).
4. D. Vocke, K. Wilson, F. Marino, I. Carusotto, E. M. Wright, T. Roger, B. P. Anderson, P. Öhberg, and D. Faccio, "Role of geometry in the superfluid flow of nonlocal photon fluids," Phys. Rev. A **94**, 013849 (2016).
5. I. Carusotto and C. Ciuti, "Quantum fluids of light," Rev. Mod. Phys. **85**, 299–366 (2013).
6. J. Klaers, J. Schmitt, F. Vewinger, and M. Weitz, "Bose-Einstein condensation of photons in an optical microcavity," Nature **468**, 545–548 (2010).
7. D. Dung, C. Kurtscheid, T. Damm, J. Schmitt, F. Vewinger, M. Weitz, and J. Klaers, "Variable potentials for thermalized light and coupled condensates," Nat. Photonics **11**, 565–569 (2017).
8. Y. Pomeau and S. Rica, "Diffraction non linéaire," C. R. Acad. Sci. Paris **317**, 1287 (1993).
9. M. Vaupel, K. Staliunas, and C. O. Weiss, "Hydrodynamic phenomena in laser physics: modes with flow and vortices behind an obstacle in an optical channel," Phys. Rev. A **54**, 880–892 (1996).
10. N. Westerberg, C. Maitland, D. Faccio, K. Wilson, P. Ohberg, and E. M. Wright, "Synthetic magnetism for photon fluids," Phys. Rev. A **94**, 023805 (2016).
11. F. Marino, M. Ciszak, and A. Ortolan, "Acoustic superradiance from optical vortices in self-defocusing cavities," Phys. Rev. A **80**, 065802 (2009).
12. I. Carusotto, "Superfluid light in bulk nonlinear media," Proc. R. Soc. London Ser. A **470**, 20140320 (2014).
13. M. C. Braidotti and C. Conti, "Quantum simulation of rainbow gravity by nonlocal nonlinearity," arXiv:1708.02623 (2017).
14. I. Fouxon, O. V. Farberovich, S. Bar-Ad, and V. Fleurov, "Dynamics of fluctuations in an optical analogue of the Laval nozzle," Europhys. Lett. **92**, 14002 (2010).
15. V. Fleurov and R. Schilling, "Regularization of fluctuations near the sonic horizon due to the quantum potential and its influence on Hawking radiation," Phys. Rev. A **85**, 045602 (2012).
16. S. Bar-Ad, R. Schilling, and V. Fleurov, "Nonlocality and fluctuations near the optical analog of a sonic horizon," Phys. Rev. A **87**, 013802 (2013).
17. W. G. Unruh, "Experimental black-hole evaporation?" Phys. Rev. Lett. **46**, 1351–1353 (1981).
18. M. Visser, "Acoustic black holes: horizons, ergospheres and Hawking radiation," Classical Quantum Gravity **15**, 1767–1791 (1998).
19. C. Barcelo, S. Liberati, and M. Visser, "Analogue gravity," Living Rev. Relativity **8**, 12 (2005).
20. C. Barcelo, S. Liberati, and M. Visser, "Analogue gravity," Living Rev. Relativity **14**, 3 (2011).
21. D. Faccio, F. Belgiorno, S. Cacciatori, V. Gorini, S. Liberati, and U. Moschella, *Analogue Gravity Phenomenology: Analogue Spacetimes and Horizons, From Theory to Experiment* (Springer, 2013), Vol. **870**.

22. T. G. Philbin, C. Kuklewicz, S. Robertson, S. Hill, F. König, and U. Leonhardt, "Fiber-optical analog of the event horizon," Science **319**, 1367–1370 (2008).
23. F. Belgiorno, S. L. Cacciatori, M. Clerici, V. Gorini, G. Ortenzi, L. Rizzi, E. Rubino, V. G. Sala, and D. Faccio, "Hawking radiation from ultrashort laser pulse filaments," Phys. Rev. Lett. **105**, 203901 (2010).
24. S. Weinfurtner, E. W. Tedford, M. C. J. Penrice, W. G. Unruh, and G. A. Lawrence, "Measurement of stimulated Hawking emission in an analogue system," Phys. Rev. Lett. **106**, 021302 (2011).
25. O. Lahav, A. Itah, A. Blumkin, C. Gordon, S. Rinott, A. Zayats, and J. Steinhauer, "Realization of a sonic black hole analog in a Bose-Einstein condensate," Phys. Rev. Lett. **105**, 240401 (2010).
26. J. Steinhauer, "Observation of quantum Hawking radiation and its entanglement in an analogue black hole," arXiv preprint arXiv:1510.00621 (2015).
27. J. Steinhauer, "Observation of self-amplifying Hawking radiation in an analogue black-hole laser," Nat. Phys. **10**, 864–869 (2014).
28. T. A. Jacobson and G. E. Volovik, "Event horizons and ergoregions in ^{3}He," Phys. Rev. D **58**, 064021 (1998).
29. D. D. Solnyshkov, H. Flayac, and G. Malpuech, "Black holes and wormholes in spinor polariton condensates," Phys. Rev. B **84**, 233405 (2011).
30. D. Gerace and I. Carusotto, "Analog Hawking radiation from an acoustic black hole in a flowing polariton superfluid," Phys. Rev. B **86**, 144505 (2012).
31. H. Nguyen, D. Gerace, I. Carusotto, D. Sanvitto, E. Galopin, A. Lemaître, I. Sagnes, J. Bloch, and A. Amo, "Acoustic black hole in a stationary hydrodynamic flow of microcavity polaritons," Phys. Rev. Lett. **114**, 036402 (2015).
32. T. Torres, S. Patrick, A. Coutant, M. Richartz, E. W. Tedford, and S. Weinfurtner, "Rotational superradiant scattering in a vortex flow," Nat. Phys. **13**, 833–836 (2017).
33. R. Penrose, "Gravitational collapse: the role of general relativity," Riv. Nuovo Cimento Soc. Ital. Fis. **1**, 252–255 (1969).
34. R. Penrose, "Gravitational collapse: the role of general relativity," Gen. Relativity Gravitation **34**, 1141–1165 (2002).
35. R. Penrose and R. Floyd, "Extraction of rotational energy from a black hole," Nature **229**, 177–179 (1971).
36. Y. B. Zel'Dovich, "Amplification of cylindrical electromagnetic waves reflected from a rotating body," Sov. Phys. JTEP **35**, 1085–1087 (1972).
37. F. Marino, "Acoustic black holes in a two-dimensional 'photon fluid'," Phys. Rev. A **78**, 063804 (2008).
38. N. Ghofraniha, C. Conti, G. Ruocco, and S. Trillo, "Shocks in nonlocal media," Phys. Rev. Lett. **99**, 043903 (2007).
39. C. Conti, A. Fratalocchi, M. Peccianti, G. Ruocco, and S. Trillo, "Observation of a gradient catastrophe generating solitons," Phys. Rev. Lett. **102**, 083902 (2009).
40. F. Dalfovo, S. Giorgini, L. P. Pitaevskii, and S. Stringari, "Theory of Bose-Einstein condensation in trapped gases," Rev. Mod. Phys. **71**, 463–512 (1999).
41. M. Richartz, A. Prain, S. Liberati, and S. Weinfurtner, "Rotating black holes in a draining bathtub: superradiant scattering of gravity waves," Phys. Rev. D **91**, 124018 (2015).
42. J. Macher and R. Parentani, "Black/white hole radiation from dispersive theories," Phys. Rev. D **79**, 124008 (2009).
43. A. Coutant and R. Parentani, "Hawking radiation with dispersion: the broadened horizon paradigm," Phys. Rev. D **90**, 121501 (2014).
44. A. Minovich, D. N. Neshev, A. Dreischuh, W. Krolikowski, and Y. S. Kivshar, "Experimental reconstruction of nonlocal response of thermal nonlinear optical media," Opt. Lett. **32**, 1599–1601 (2007).
45. D. F. A. Faccio and D. E. F. Vocke, "Rotating black hole geometries in a two-dimensional photon superfluid," https://doi.org/10.17861/aee7b4b0-df87-4f22-8565-badb5d407567.